

6-13-2016

# Proportions of Convective and Stratiform Precipitation Revealed in Water Isotope Ratios

Pradeep K. Aggarwal  
*International Atomic Energy Agency*

Ulrike Romatschke  
*International Atomic Energy Agency*


Luis Araguas-Araguas  
*International Atomic Energy Agency*

Dagnachew Belachew  
*International Atomic Energy Agency*

Fred J. Longstaffe  
*The University of Western Ontario, flongsta@uwo.ca*

*See next page for additional authors*

Follow this and additional works at: <https://ir.lib.uwo.ca/earthpub>

 Part of the [Geochemistry Commons](#), [Hydrology Commons](#), and the [Water Resource Management Commons](#)

---

## Citation of this paper:

Aggarwal, Pradeep K.; Romatschke, Ulrike; Araguas-Araguas, Luis; Belachew, Dagnachew; Longstaffe, Fred J.; Berg, Peter; Schumacher, Courtney; and Funk, Aaron, "Proportions of Convective and Stratiform Precipitation Revealed in Water Isotope Ratios" (2016). *Earth Sciences Publications*. 13.  
<https://ir.lib.uwo.ca/earthpub/13>

---

**Authors**

Pradeep K. Aggarwal, Ulrike Romatschke, Luis Araguas-Araguas, Dagnachew Belachew, Fred J. Longstaffe, Peter Berg, Courtney Schumacher, and Aaron Funk

# Proportions of Convective and Stratiform Precipitation Revealed in Water Isotope Ratios

Pradeep K. Aggarwal<sup>1\*</sup>, Ulrike Romatschke<sup>1</sup>, Luis Araguas-Araguas<sup>1</sup>, Dagnachew Belachew<sup>1</sup>,  
Frederick J. Longstaffe<sup>2</sup>, Peter Berg<sup>3</sup>, Courtney Schumacher<sup>4</sup>, Aaron Funk<sup>4</sup>

<sup>1</sup>Isotope Hydrology Section, International Atomic Energy Agency, Vienna, Austria

<sup>2</sup>Department of Earth Sciences, The University of Western Ontario, London, ON, Canada

<sup>3</sup>Hydrology Unit, Swedish Meteorological and Hydrological Institute, Norrköping, Sweden

<sup>4</sup>Department of Atmospheric Sciences, Texas A&M University, College Station, TX, USA

\* Corresponding Author (+43 1 2600 21735; p.aggarwal@iaea.org)

Submitted to: **Nature Geoscience**

Original:	April 21, 2015
Re-submitted:	January 25, 2016
Revised:	May 3, 2016

1 Tropical and midlatitude precipitation is fundamentally of two types, spatially-limited and  
2 high-intensity convective or widespread and lower-intensity stratiform, owing to  
3 differences in vertical air motions and microphysical processes governing rain formation.  
4 These processes are difficult to observe or model and precipitation partitioning into rain  
5 types is critical for understanding how the water cycle responds to climate changes. Here,  
6 we combine two independent data sets – convective and stratiform precipitation fractions,  
7 derived from the Tropical Rainfall Measuring Mission satellite or synoptic cloud  
8 observations, and stable isotope and tritium compositions of surface precipitation, derived  
9 from a global network – to show that isotope ratios reflect rain type proportions and are  
10 negatively correlated with stratiform fractions. Condensation and riming associated with  
11 boundary layer moisture produces higher isotope ratios in convective rain, along with  
12 higher tritium when riming in deep convection occurs with entrained air at higher  
13 altitudes. Based on our data, stable isotope ratios can be used to monitor changes in the  
14 character of precipitation in response to periodic variability or changes in climate. Our  
15 results also provide observational constraints for an improved simulation of convection in  
16 climate models and a better understanding of isotope variations in proxy archives, such as  
17 speleothems and tropical ice.

Stable isotope ratios ( $\delta^{18}\text{O}$ ,  $\delta^2\text{H}$ ; Methods) have long been observed to be different in precipitation from different types of clouds, such as those producing convective showers versus those producing frontal, continuous rain<sup>1-4</sup>. Recent studies<sup>5-8</sup> have observed lower  $\delta^{18}\text{O}$  in precipitation from stratiform clouds, in hydrologically more organized cloud systems, or when a “bright band” occurs in vertical radar reflectivity. These observations have all been interpreted using a Rayleigh distillation concept<sup>1-9</sup>, wherein adiabatic cooling of an air mass results in successive condensation (rainout) with progressively lower  $\delta^{18}\text{O}$  of precipitation at lower temperatures in midlatitudes or increasing rain amount (‘amount effect’) in the tropics. Existing interpretations of the ‘amount effect’ consider it to result from the low  $\delta^{18}\text{O}$  of deep convective rain forming at higher altitudes and a lack of isotopic exchange with near surface moisture due to rapid fall velocities<sup>1-4</sup>, or from in-cloud re-evaporation of rain and isotopic exchange with  $^{18}\text{O}$ -depleted moisture at low altitudes<sup>5-6,9</sup>. Likewise, sub-cloud evaporation and isotopic exchange with ambient moisture are described as accentuating the ‘amount effect’ by increasing  $\delta^{18}\text{O}$  when precipitation amounts are low, particularly under drier and warmer conditions<sup>1-9</sup>. Although simulations of isotope distributions in global climate models (GCMs) differentiate between convective and non-convective precipitation, their isotope schemes are based essentially on different variations of the Rayleigh concept<sup>3,5,7,9-13</sup>. A comprehensive framework that adequately explains observed isotope distributions in tropical and midlatitude precipitation, however, is still lacking<sup>4</sup>.

A key assumption underpinning current interpretations of precipitation isotope distribution is that a change in  $\delta^{18}\text{O}$  of precipitation directly represents a change in one or more of the parameters that may influence the isotopic composition, such as moisture source, temperature, rainout, or post-condensation isotope exchange. It is important to note that in spite of potentially large differences in these parameters,  $\delta^{18}\text{O}$  of 50°N to 50°S precipitation normally

has a range of  $\sim -30$  to  $0\text{‰}$  (*ref. 16*), and most or all of this variability may be observed in single or consecutive storm events<sup>1,6,8,14,15</sup>. Recently, precipitation  $\delta^{18}\text{O}$  has been correlated globally with a single climate parameter<sup>17</sup> (atmospheric moisture residence time), which reflects the degree of hydrological organization or structures of precipitating clouds. Tropical and midlatitude precipitation sampled on the Earth's surface almost always consists of varying proportions of two fundamental rain types<sup>18-23</sup> – stratiform and convective – with significantly different characteristics of temporal and spatial variability<sup>20-25</sup> arising from differences in cloud vertical air motions and microphysical processes during hydrometeor formation, growth, and descent to the surface. These differences in rain formation impart characteristic isotope signatures (as we will discuss below) and changing proportions of convective and stratiform rain types may primarily be responsible for precipitation isotope variability.

### **Rain type fractions and stable isotope ratios**

Figures 1a and 1b show mean monthly  $\delta^{18}\text{O}$  with respect to stratiform rain fractions and precipitation amount from 28 tropical and two midlatitude locations (Table 1). We retrieved monthly stratiform fractions (1998-2014) from the TRMM Precipitation Radar 2A25 (version 7) data product<sup>21,26,27</sup> and (for midlatitudes) synoptic cloud observations<sup>24</sup> (Methods). Monthly  $\delta^{18}\text{O}$  and precipitation amounts are from the IAEA/WMO global network of isotopes in precipitation (GNIP) database<sup>16</sup> (Methods). The locations listed in Figure 1 span a broad latitudinal range ( $50^{\circ}\text{N}$ – $21^{\circ}\text{S}$ ) and hydro-meteorological conditions: small islands in the Indian, Pacific, or Atlantic oceans, coastal or inland continental, sea-level to  $\sim 3000$  m altitude, and low to high, mean annual precipitation amounts ( $\sim 166$ – $5000$  mm) or surface air temperatures ( $\sim 7$ – $29^{\circ}\text{C}$ ).

66 The  $\delta^{18}\text{O}$  increases with decreasing stratiform fractions (Fig. 1a) and a regression  
67 including all locations indicates a strong negative correlation ( $R^2 \approx 0.6$ ;  $p < 0.0001$ ). This  
68 correlation probably would be stronger, if not for somewhat independent variability and  
69 uncertainty in rain fraction and isotope data. TRMM satellite coverage is limited to 0–2 swaths  
70 per day in a  $2.5^\circ$  grid and may include only a few of the precipitation days in a month<sup>21,26,27</sup>.  
71 Some of this variability is reduced by taking climatological means, but probably not in relation  
72 to  $\delta^{18}\text{O}$  because of the different spatial scales (point location versus a  $2.5^\circ$  grid cell) of the  
73 isotope versus TRMM data. The uncertainty in estimated stratiform fraction is also greater  
74 when shallow rain is significant and when rain amounts are low<sup>21,27</sup>. Rain types based on cloud  
75 observations may overestimate the stratiform fractions (Methods). Additionally, isotope data  
76 can be biased towards that of stratiform rain because a fixed location for isotope sampling may  
77 not experience all convective rainfall events owing to the limited spatial extents of convective  
78 clouds.

79  $\delta^{18}\text{O}$  – precipitation amount correlation is quite variable (Fig. 1b), even though  
80 at each tropical location there is a general trend of decreasing  $\delta^{18}\text{O}$  with increasing precipitation.  
81 Stratiform fractions and precipitation amount (Fig. 1c) show an opposite correlation compared  
82 to  $\delta^{18}\text{O}$  and even low amounts of precipitation have low  $\delta^{18}\text{O}$  when the stratiform fraction is  
83 high. More importantly, a significant increase in tropical monthly precipitation (~400–900 mm)  
84 occurs with a limited  $\delta^{18}\text{O}$  variability that is consistent with the narrow range in stratiform  
85 fractions.

### 86 **Convective – stratiform isotope differences**

88 The low and high  $\delta^{18}\text{O}$ , respectively, of stratiform and convective rain are consistent  
89 with dynamical and microphysical conditions of rain formation (Fig. 2). In stratiform clouds

(nimbostratus), vertical air motions are weak<sup>18-23</sup> with mean upward air velocity ( $\sim 0.2 \text{ m s}^{-1}$ ) much lower than typical ice and snow terminal fall velocity ( $\sim 1 \text{ m s}^{-1}$ ). Condensation nuclei (ice particles) form or are introduced near cloud tops and grow, initially by vapor deposition (diffusion) and later by aggregation, while falling slowly towards the surface<sup>18-23</sup>. Below the freezing level, melting occurs in an  $\sim 500 \text{ m}$  thick layer<sup>18,19</sup> (‘bright band’ observed in vertical radar reflectivity profiles) and as raindrops fall further, they may partially evaporate, under conditions of subsidence, or grow by accretion and coalescence, under conditions of uplift<sup>18,19</sup>. The time for condensation, growth and rainfall for stratiform precipitation is about 1-3 hours<sup>19</sup>.

Hydrometeor growth by vapor diffusion above the freezing level, where tropospheric moisture would have a  $\delta^{18}\text{O}$  of  $\sim -50$  to  $-40\text{‰}$  (*ref.* 28), isotopic homogenization in the melting layer, and equilibration with lower altitude moisture<sup>29</sup> as relatively small rain drops<sup>19</sup> (on average  $\sim 1 \text{ mm}$  in diameter) fall slowly to the surface, all would result in low  $\delta^{18}\text{O}$  of stratiform rain. Because of the isotopic exchange below the melting level, near-surface temperature would have a greater influence, resulting in a range of  $\delta^{18}\text{O}$ . When the melting level is near or at the ground surface ( $\sim 1 \text{ km}$  or lower), as in midlatitude winters, limited or negligible exchange with ambient moisture<sup>3,9,10,28,29</sup> would produce relatively more negative  $\delta^{18}\text{O}$  of stratiform precipitation.

In contrast, condensation particles in convective clouds (cumulus or cumulonimbus) form near the cloud base<sup>18-23</sup> and grow as they are lifted in strong updrafts ( $1\text{--}10 \text{ m s}^{-1}$ ). The time from initiation of condensation to rainfall in a single convective cell may be as little as thirty minutes<sup>19</sup>. When convection is shallow, precipitation forms by ‘warm’ processes<sup>19-21</sup>, wherein condensation occurs below the freezing level and rain drops grow by collision and coalescence. In deep convection, condensation nuclei form as ice particles just above the freezing level, and grow rapidly in updrafts by riming as super-cooled water (mostly from the



planetary boundary layer) is frozen at successively higher altitudes<sup>19-23</sup>. Entrainment of surrounding air above the freezing level may also contribute minor proportions of moisture for riming growth in convective updrafts<sup>19</sup>. As particles become large enough (e.g. graupel) to overcome upward air motion, they descend in strong downdrafts, melt rapidly below the 0°C level, as opposed to a ‘melting layer’ in stratiform precipitation, and fall as large rain drops (>2 mm diameter) without significant evaporation or growth<sup>19-23</sup>.

Convective updrafts are fed by boundary layer moisture, with  $\delta^{18}\text{O}$  similar to that of ocean evaporation ( $\sim -12$  to  $-10\text{‰}$ ), particularly in oceanic or coastal locations, and slightly lower more inland depending upon the contribution from evaporated soil moisture<sup>4</sup>. The liquid-vapor isotope fractionation<sup>4,9</sup> is  $\sim 10.7 - 9.8\text{‰}$  (0 to 10°C) and shallow convective or ‘warm’ rain would likely have a  $\delta^{18}\text{O}$  that is about  $-1 \pm 1 \text{‰}$ . In deep convective precipitation, ice particles from boundary layer moisture just above the freezing level would have  $\delta^{18}\text{O}$  of  $\sim 0\text{‰}$  or higher as ice-vapor isotope fractionation<sup>9</sup> (at 0 to  $-10^\circ\text{C}$ ) is  $\sim 4\text{‰}$  greater than that for liquid-vapor. In addition, depending upon the nature of ice particle surfaces, the kinetic isotope fractionation between ice-vapor or ice-liquid could be even larger<sup>30</sup>. As ice particles are lifted in updrafts, further accretion (riming) of supercooled boundary layer moisture would also result in relatively higher  $\delta^{18}\text{O}$ . Entrained environmental air at higher altitudes may have a low  $\delta^{18}\text{O}$ , but because of its low moisture content, it is unlikely to significantly decrease the  $\delta^{18}\text{O}$  of hydrometeors<sup>31</sup>. Ice particles or graupel falling in downdrafts will melt beneath the 0°C level and the large size and fall velocity<sup>19</sup> ( $\sim 5$  to  $10 \text{ m s}^{-1}$ ) of the rain drops will inhibit isotopic exchange with ambient moisture<sup>29,31</sup>, preserving the high  $\delta^{18}\text{O}$  acquired during ice and riming growth in updrafts. This is consistent with precipitation tritium ( $^3\text{H}$ ) contents (see below).

### **Tritium in convective rain**

Differences in ice formation, growth, and melting in convective and stratiform clouds resulting in different  $\delta^{18}\text{O}$  are evident also in the maximum height of high reflectivity, 40-dBZ echo recorded by TRMM precipitation radar<sup>19,32,33</sup>. High reflectivity indicates large ice particles (i.e., graupel) above the 0°C level (~5 km in the tropics) lifted in strong updrafts, a melting layer of ice particles just below the 0°C level exhibiting a bright band characteristic of stratiform clouds, or intense rain beneath the 0°C level as seen commonly over the oceans<sup>19,32</sup>. Figures 3a and 3b show the  $\delta^{18}\text{O}$  and stratiform rain fractions for tropical stations with respect to the 40-dBZ echo height. We could not access similar data for Vienna and Krakow because they are northward of the TRMM satellite orbital extent. High  $\delta^{18}\text{O}$  with low stratiform fractions occurs with echo heights >5 km (i.e., deep convection) or <~1 km (warm rain). For higher stratiform fractions (>~30%), a wider range of lower  $\delta^{18}\text{O}$  occurs with the 40-dBZ echo at ~2-4 km.

Figures 4a and 4b show  $^3\text{H}$  for selected tropical and midlatitude locations with respect to stratiform fractions and  $\delta^{18}\text{O}$ . Tritium contents are also derived from the GNIP database<sup>16</sup> and are expressed in tritium units (1TU =  $10^{-18}$   $^3\text{H}/\text{H}$ ; Methods). As noted earlier, riming growth in deep convective updrafts may include entrained moisture at higher altitudes (~6-8 km) where  $^3\text{H}$  contents are expected to be very high<sup>29,34</sup> (>~ $10^4$  TU) compared to those near surface (presently ~5 TU or less). Even minor amounts of this high altitude moisture in hydrometeors (~5% of total water budget) would substantially increase precipitation  $^3\text{H}$  contents<sup>23</sup>, resulting in a positive  $^3\text{H} - \delta^{18}\text{O}$  correlation. Isotopic exchange and equilibration at lower altitudes (as in stratiform rain) will decrease precipitation  $^3\text{H}$  contents to ambient levels<sup>29,34</sup>.

At Dhaka and New Delhi, the 40-dBZ echo heights are >~6 km (Fig. 3). Deep convection with similar echo heights is also known to occur at Vienna and Krakow<sup>35</sup>. All of these locations show an increasing  $^3\text{H}$  with decreasing stratiform fraction or increasing  $\delta^{18}\text{O}$

(Figs. 4a, 4b), indicating that higher  $\delta^{18}\text{O}$  did not result from isotopic exchange or in-cloud rain re-evaporation at lower altitudes. Lower  $^3\text{H}$  and a lack of  $^3\text{H} - \delta^{18}\text{O}$  correlation at Bogota, Bangkok and Hong Kong (Figs. 4a, 4b) are consistent with lower heights of deep convection and higher stratiform fractions (Fig. 3) at these locations.

### **Isotope variability and character of precipitation**

Variable convective and stratiform fractions are an integral feature of precipitating clouds in the tropics and midlatitudes<sup>18-24</sup> where mesoscale convective systems and extra-tropical cyclones produce most of the precipitation<sup>19</sup>. Average annual stratiform fractions (on a volume basis) are ~35-55% in the tropics<sup>21</sup> and are higher in the midlatitudes<sup>19,35</sup>. Smaller, less organized convective systems have much lower stratiform fractions. Substantial variability in rain type fractions ranging from near zero to nearly all stratiform rain may occur during storm events both in the tropics and midlatitudes<sup>1,6,8,15</sup>. Complex patterns<sup>4-8</sup> of precipitation  $\delta^{18}\text{O}$  decreasing, increasing, and then decreasing again with time are commonly observed<sup>4-8</sup> during storm events and may easily result from successive storms with stratiform precipitation trailing convective<sup>19,36</sup>. A progressive decrease, increase or no change in  $\delta^{18}\text{O}$  with time<sup>5,6,14,15</sup> may occur when stratiform precipitation trails, leads, or overlaps convective precipitation<sup>36</sup>.

The  $\delta^{18}\text{O}$  – stratiform fraction correlation shown in Figure 1 for monthly data is found also at storm event or interannual time scales. Recent measurements of isotope ratios in the equatorial Indian Ocean<sup>4,15</sup> and in California, USA<sup>8</sup> both indicate that  $\delta^{18}\text{O}$  is low ( $\sim -20\text{‰}$ ) when precipitation is dominantly stratiform and high ( $\sim 0\text{‰}$ ) when it is mostly convective. Significant interannual variability occurs in response to regional or global phenomenon, such as the El Niño–Southern Oscillation (ENSO)<sup>37</sup>, and the character of precipitation is affected differently across the Pacific<sup>21</sup>, with lower stratiform fractions in the west (e.g. Darwin, 130°E)

and higher in the east (e.g. Bellavista, 90°W). These opposite trends are seen in the mean annual isotope ratios for 1998, a strong El Niño year (positive ENSO index), compared to average values for 1999-2001. At Darwin, 1998 precipitation had lower stratiform fractions (29%; average 33%) and higher  $\delta^{18}\text{O}$  (−4.9‰; average −6.0‰), while at Bellavista, fractions were higher (49%; average 30%) and  $\delta^{18}\text{O}$  lower (−5.5‰; average −2.9‰).

The negative correlation between  $\delta^{18}\text{O}$  and stratiform rain fractions (Fig. 1a) is also consistent with the previously observed positive correlation between  $\delta^{18}\text{O}$  and moisture residence time<sup>17</sup> because residence time would be lower, and stratiform fractions higher, in well-organized, mesoscale convective systems and extra-tropical cyclones<sup>19,21</sup>.

We conclude that  $\delta^{18}\text{O}$  in tropical and midlatitude precipitation reflects the proportions of convective and stratiform rain. Routine measurements of stable isotopes and tritium in sub-daily or daily precipitation will help to better understand short-term variability in cloud dynamics responsible for changes in rain fractions. In addition, isotope data could be used to evaluate the relative importance of ‘warm’ process rain as a contribution to total precipitation, as well as an independent, diagnostic tool to monitor variability in, and climate change impacts on, the character of precipitation<sup>38,39</sup>.

Precipitation partitioning based on isotope distributions should help to improve climate models<sup>25</sup> and the simulation of convection by providing observational constraints for tropospheric heating profiles and rain types<sup>18-22,41</sup>. Isotope schemes in GCMs for convective and stratiform precipitation that are consistent with microphysical processes depicted in Figure 2 should lead to model results being robust across temporal and spatial scales. Our results also suggest that, similar to variations in modern precipitation, annual average  $\delta^{18}\text{O}$  recorded in proxy archives of paleo-precipitation<sup>41</sup>, such as speleothems and tropical ice, should reflect a change in the proportions of convective and stratiform precipitation. Lower or higher  $\delta^{18}\text{O}$ , for

example, may result from higher or lower stratiform fractions, which may or may not coincide with wetter or drier conditions (Fig. 1). A re-examination of proxy isotope data in this light should facilitate the development of more reliable models of past and future climate change impacts on the water cycle.

## References

1. Dansgaard, W. The abundance of O<sup>18</sup> in atmospheric water and water vapour. *Tellus* **5**, 461-469 (1953).
2. Dansgaard, W. Stable isotopes in precipitation. *Tellus* **16**, 436–468 (1964).
3. Gedzelman, S. D. & Lawrence, J. R. The isotopic composition of cyclonic precipitation. *J. Appl. Meteorol.* **21**, 1385–1404 (1982).
4. Gat, J. R. Oxygen and hydrogen isotopes in the hydrologic cycle. *Ann. Rev. Earth Planet. Sci.* **24**, 225-262 (1996).
5. Risi, C. *et al.* Evolution of the stable water isotopic composition of the rain sampled along Sahelian squall lines. *Quarterly Jour. Royal Meteo. Soc.* **136.S1**, 227-242 (2010).
6. Kurita, N. *et al.* Intraseasonal isotopic variation associated with the Madden-Julian Oscillation. *J. Geophys. Res* **116**, D24101 (2011).
7. Gao, J. *et al.* What controls precipitation  $\delta^{18}\text{O}$  in the southern Tibetan Plateau at seasonal and intra-seasonal scales? A case study at Lhasa and Nyalam. *Tellus-B*, **65**, 21043-21055 (2013).
8. Coplen, T. B. *et al.* Categorisation of northern California rainfall for periods with and without a radar brightband using stable isotopes and a novel automated precipitation collector. *Tellus B*, **67**, 28574 (2015).
9. Jouzel, J. Water stable isotopes: Atmospheric composition and applications in polar ice core studies, *Treatise on Geochemistry* 2<sup>nd</sup> Ed., 213-256 (2014)
10. Gedzelman, S. D. & Arnold, R. Modeling the isotopic composition of precipitation. *J. Geophys. Res.* **99**, 10455-10471 (1994).
11. Kurita, N. Water isotopic variability in response to mesoscale convective system over the tropical ocean. *J. Geophys. Res.* **118**, 1-15 (2013).
12. Sturm, C., Zhang, Q. & Noone, D. An introduction to stable water isotopes in climate models: benefits of forward proxy modelling for paleoclimatology. *Clim. Past* **6**, 1: 115-129 (2010).

- 254  
255 13. Sutanto, S. J. *et al.* Atmospheric processes governing the changes in water isotopologues during  
256 ENSO events from model and satellite measurements. *J. Geophys. Res.* **120**, 6712-6729 (2015).  
257  
258 14. Moerman, J. W. *et al.* Diurnal to interannual rainfall  $\delta^{18}\text{O}$  variations in northern Borneo driven  
259 by regional hydrology. *Earth Planet. Sci. Lett.* **369**, 108-119 (2013).  
260  
261 15. Fudeyasu, H. *et al.* Effects of large-scale moisture transport and mesoscale processes on  
262 precipitation isotope ratios observed at Sumatera, Indonesia *J. Meteorol. Soc. Jpn.* **89**, 49-59  
263 (2011).  
264  
265 16. Aggarwal, P. K. *et al.* New capabilities for studies using isotopes in the water cycle. *Eos Trans.*  
266 *AGU* **88**, 537 (2007).  
267  
268 17. Aggarwal, P. K. *et al.* Stable isotopes in global precipitation: A unified interpretation based on  
269 atmospheric moisture residence time. *Geophys. Res. Lett.* **39**, L11705 (2012).  
270  
271 18. Houze, R. A. Jr. Stratiform precipitation in regions of convection: A meteorological  
272 paradox? *Bull. Amer. Met. Soc.* **78**, 2179-2196 (1997).  
273  
274 19. Houze, R. A. Jr. *Cloud dynamics*. International Geophysics Series, vol. 104, Academic Press,  
275 (2014).  
276  
277 20. Houze, R. A. Jr. Structures of atmospheric precipitation systems: A global survey." *Radio*  
278 *Science* **16**, 671-689 (1981).  
279  
280 21. Schumacher, C. & Houze, R. A. Jr. Stratiform rain in the tropics as seen by the TRMM  
281 precipitation radar. *Jour. Climate* **16**, 1739-1756 (2003).  
282  
283 22. Stith, J. L. *et al.* Microphysical observations of tropical clouds. *J. Appl. Meteorol.* **41**, 97-117  
284 (2002).  
285  
286 23. Steiner, M. & Smith, J. A. Convective versus stratiform rainfall: An ice-microphysical and  
287 kinematic conceptual model. *Atmos. Res.* **47**, 317-326 (1998).  
288  
289 24. Berg, P. *et al.* Strong increase in convective precipitation in response to higher temperatures  
290 *Nat. Geosci.* **6**, 181-185 (2013).  
291  
292 25. Prein, F. *et al.* A review on regional convection-permitting climate modeling: Demonstrations,  
293 prospects, and challenges *Rev. Geophys.*, **53**, 323-361 (2015)  
294  
295 26. Liu, C. *et al.* A cloud and precipitation feature database from nine years of TRMM  
296 observations. *J. Appl. Meteorol. Clim.* **47**, 2712-2728 (2008).  
297  
298 27. Funk, A., Schumacher, C. & Awaka, J. Analysis of Rain Classifications over the Tropics by  
299 Version 7 of the TRMM PR 2A23 Algorithm. *J. Meteorol. Soc. Jpn.* **91**, 257-272 (2013).  
300

28. Ehhalt, D. H., Rohrer, F. & Fried, A. Vertical profiles of HDO/H<sub>2</sub>O in the troposphere. *J. Geophys. Res.* **110**, 7351-7366 (2005).
29. Bolin, B. On the use of tritium as a tracer for water in nature. *Proc. Second United Nations Intl. Conf. Peaceful Uses of Atomic Energy.* **18**, 336-343 (1959).
30. Nelson, J. Theory of isotopic fractionation on faceted ice crystals. *Atmos. Chem. Phys.* **11**, 11351–11360 (2011).
31. Knight, C. A. *et al.* Radial and tangential variation of deuterium in hailstones *Jour. Atmos. Sci.* **32**, 1990-2000 (1975).
32. Zipser, E. J. *et al.* Where are the most intense thunderstorms on Earth? *Bull. American Meteor. Soc.* **87**, 1057-1071 (2006).
33. Romatschke, U. & Houze, R. A. Jr. Characteristics of precipitating convective systems in the South Asian monsoon. *J. Hydrometeorol.* **12**, 3–26 (2011).
34. Ehhalt, D. H. Vertical profiles and transport of HTO in the troposphere. *J. Geophys. Res.* **76**, 7351-7367 (1971).
35. Liu, C. & Zipser, E. J. The global distribution of largest, deepest, and most intense precipitation systems. *Geophys. Res. Lett.* **42**, 3561-3595 (2015).
36. Parker, M. D. & Johnson, R. H. Organizational modes of midlatitude mesoscale convective systems *Monthly Weath. Rev.* **128**, 3413-3436 (2000).
37. Trenberth, K. E. & Caron J. M. The Southern Oscillation revisited: Sea level pressures, surface temperatures, and precipitation. *J. Clim.* **13**, 4358-4365 (2000).
38. Hartmann, D. L. *et al.* Observations: Atmosphere and Surface In: Climate Change 2013: The Physical Science Basis. Cambridge University Press, Cambridge, United Kingdom and New York, NY, USA (2013).
39. Westra, S. *et al.* Future changes to the intensity and frequency of short-duration extreme rainfall. *Rev. Geophys.* **52**, 522-555 (2014).
40. Houze, R. A. Jr. Observed structure of mesoscale convective systems and implications for large-scale heating. *Q. J. R. Meteorol. Soc.* **115**, 425-461 (1989).
41. Dayem, K. E. *et al.* Lessons learned from oxygen isotopes in modern precipitation applied to interpretation of speleothem records of paleoclimate from eastern Asia *Earth Planet. Sci. Lett.* **295**, 219-230 (2010).

**Author contributions:** PKA initiated the project and wrote the paper; UR, DB, CS and AF provided TRMM data; LAA processed isotope and related data; PB contributed cloud-based stratiform fractions; all authors contributed to data evaluation and commented on the manuscript.

**Competing interests:** There are no competing interests.

## **METHODS**

### **Stratiform fractions**

*Tropical locations:* Stratiform rain fractions were calculated using NASA's TRMM PR 2A23 (rain type classification) and 2A25 (attenuation correction) orbital data products for 1998-2014. For each major rain type (stratiform, deep convective, shallow convective), radar reflectivity data was binned by latitude, longitude and height with a reflectivity bin spacing of 2 dBZ and spatial bin spacing of 2.5° by 2.5° from 35°N to 35°S. Rainfall was estimated at each grid point using PR data measured ~2 km above mean ground level height. Stratiform and convective conditional rain rates were estimated from mean radar reflectivity ( $\geq 18$  dBZ) using 2A25 V7 initial stratiform and convective Z-R relations<sup>27</sup>. Unconditional rain rates could then be estimated using the probability of rainfall at each grid point based on TRMM PR observations. Stratiform rainfall fraction here is defined as the ratio of stratiform volumetric rainfall to total volumetric rainfall or the ratio of unconditional rain rates.

In TRMM rain type classification, rain is either stratiform or convective. The "other" pixels that the algorithm predicts are raining are very small in count (1.7% of all raining pixels) and likely don't contribute much to rainfall near the surface; this rain appears to mostly exist at higher levels and has an anvil appearance<sup>27</sup>. These pixels are not used in our stratiform-convective rain calculations. Therefore, for our purposes here, 0% stratiform is essentially 100% convective with the exception of 'no-rain' cases.



369 *Midlatitude locations:* For Vienna and Krakow, average monthly stratiform fractions for the period  
370 1998-2014 were calculated from 3-hourly synoptic cloud observations in the MIDAS data base<sup>24</sup>:  
371 ([http://badc.nerc.ac.uk/view/badc.nerc.ac.uk\\_\\_ATOM\\_\\_dataent\\_ukmo-midas](http://badc.nerc.ac.uk/view/badc.nerc.ac.uk__ATOM__dataent_ukmo-midas)). Precipitation is  
372 classified as convective when cumulus or cumulonimbus type clouds are present, and as stratiform  
373 when stratus or nimbostratus are present. Conditions with mixed cloud types are separated in the  
374 statistics. A day-night bias in the synoptic data could potentially affect the results. The stratiform  
375 fraction is deemed more reliable and is derived as the amount of precipitation classified as stratiform  
376 divided by total precipitation. Sensitivity studies with convective fraction derived as the ratio of the  
377 amount of convective precipitation to total precipitation yield similar result. We note, however, that the  
378 sum of convective and stratiform fractions generally is much less than 100% for many samples, giving  
379 rise to a greater uncertainty in estimated fractions.

380

### 381 **Stable isotopes, precipitation amount and tritium**

382 Stable isotope abundances in precipitation are expressed as  $\delta^{18}\text{O}$  or  $\delta^2\text{H} = (\text{Rx}/\text{Rstd} - 1) \times 1000$ ,  
383 where R is the  $^{18}\text{O}/^{16}\text{O}$  or  $^2\text{H}/\text{H}$  ratio in a sample (x) or standard (std) and the isotopic standard is  
384 VSMOW. Our analysis uses only oxygen isotope ratios ( $\delta^{18}\text{O}$ ) because hydrogen isotope ratios are  
385 proportional to those of oxygen<sup>1,2</sup>.

386 □□□□  $\delta^{18}\text{O}$  and precipitation amount were retrieved from the global network of isotopes in  
387 precipitation (GNIP) database<sup>16</sup> [http://www-naweb.iaea.org/napc/ih/IHS\\_resources\\_gnip.html](http://www-naweb.iaea.org/napc/ih/IHS_resources_gnip.html). Tropical  
388 locations in the 30°N – 30°S latitude range, with a minimum of four consecutive years of isotope data  
389 in the 1998-2014 period, were selected. Isotope data from Jambi and Bukit stations in Indonesia were  
390 obtained within the framework of “Daily basis precipitation sampling network for water isotope  
391 analysis” at the Institute of Observational Research for Global Change, Japan Agency for Marine-Earth  
392 Science and Technology, by N. Kurita and K. Ichiyanagi. In addition, data for two midlatitude

393 locations (Vienna and Krakow) were retrieved from the GNIP database. Monthly means were used to  
394 calculate long-term arithmetic means (unweighted) for months with more than 50 mm precipitation  
395 (Table 1), except for Ascension Island, Vienna and Krakow, where all months with consistent data over  
396 multiple years were used.

397 Tritium ( $^3\text{H}$ ) is reported in Tritium Units (TU) where  $1 \text{ TU} = 10^{-18} \text{ } ^3\text{H}/\text{H}$ . Analyses of water  
398 samples for tritium is carried out using ultra-low level liquid scintillation counters after electrolytical  
399 enrichment (or concentration) of tritium from a large sample by electrolysis. Current analytical  
400 methods allow a typical uncertainty in tritium analysis of about  $\pm 0.1$  to  $\pm 0.5$  TU. Tritium is produced in  
401 the stratosphere by cosmic ray spallation and reaches the troposphere by moisture ‘leakage’ or  
402 exchange and its abundance decreases towards the Earth’s surface<sup>20,26</sup>. In addition, a latitudinal  
403 gradient (decreasing  $^3\text{H}$  contents towards the equator) exists due to the fact that stratospheric exchange  
404 occurs mostly in mid to high latitudes<sup>20,21</sup>. Stratospheric  $^3\text{H}$  injection by thermo-nuclear bomb tests  
405 before 1963 swamped the cosmogenic production and tropospheric tritium increased by orders of  
406 magnitude. This ‘bomb’ tritium was gradually washed out of the stratosphere and troposphere by the  
407 1990s, but vertical differences in tropospheric  $^3\text{H}$  contents remained.

408 Precipitation  $^3\text{H}$  contents were also retrieved from the GNIP database for 1998–2012, except for  
409 New Delhi where data were available for 1964–1978. During this period, atmospheric  $^3\text{H}$  was declining  
410 rapidly due to the wash out of ‘bomb’ tritium<sup>34</sup>. As a result, absolute  $^3\text{H}$  values for New Delhi cannot  
411 be compared directly with other locations. The  $^3\text{H} - \delta^{18}\text{O}$  correlations for New Delhi shown in Fig. 4b  
412 are based on data for both isotopes from the same time period (1964-1978), but are shown for smaller  
413 time intervals after normalization by the average for each period so that the correlation is not masked  
414 by declining concentrations. The lower  $^3\text{H}$  at Dhaka compared to Vienna or Krakow reflects the  
415 latitudinal gradient in tropospheric  $^3\text{H}$  concentration because the stratosphere-troposphere exchange

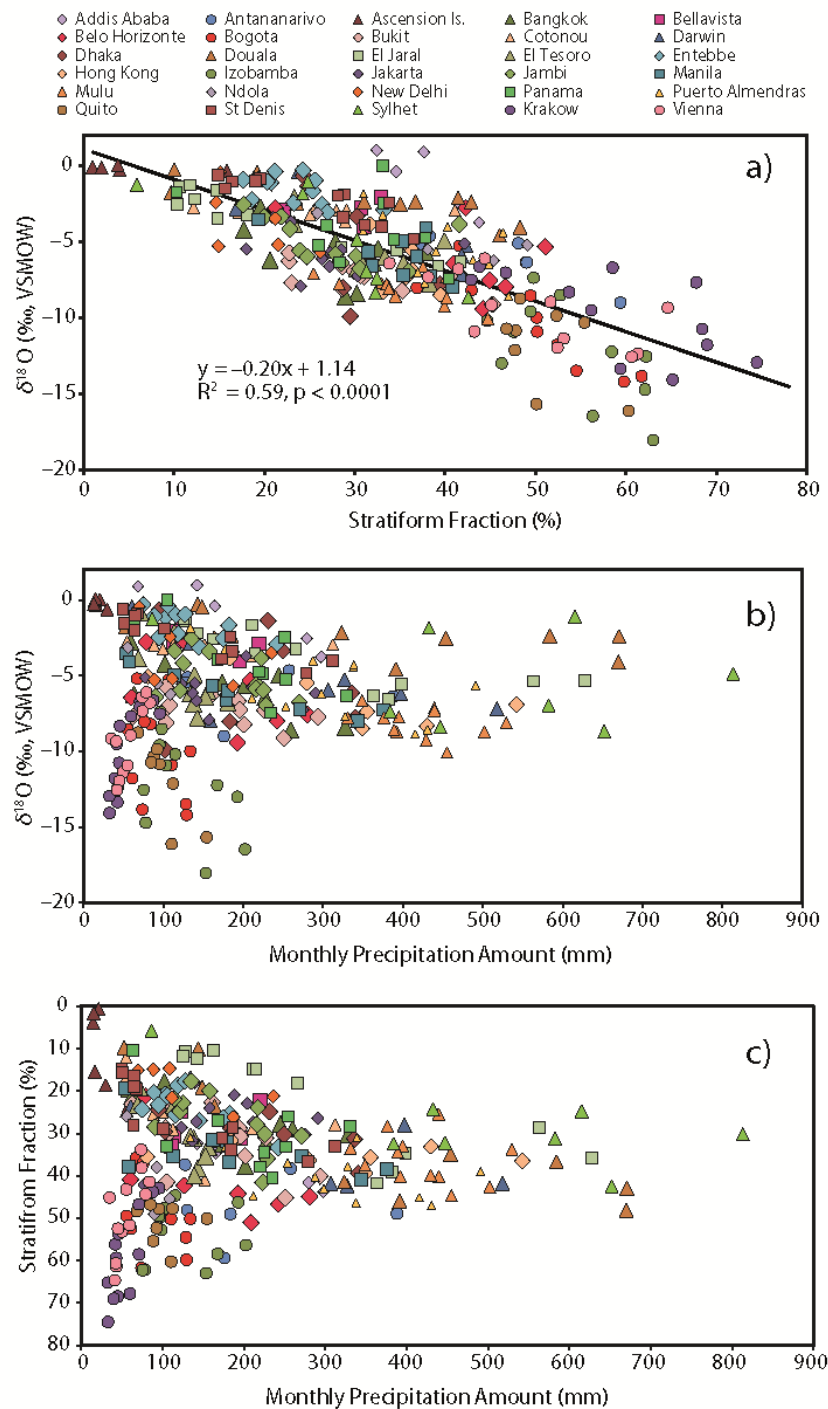
416 that brings tritium to the troposphere occurs mostly at higher latitudes<sup>29,34</sup>, as well as differences in the  
417 height of convective entrainment.

418

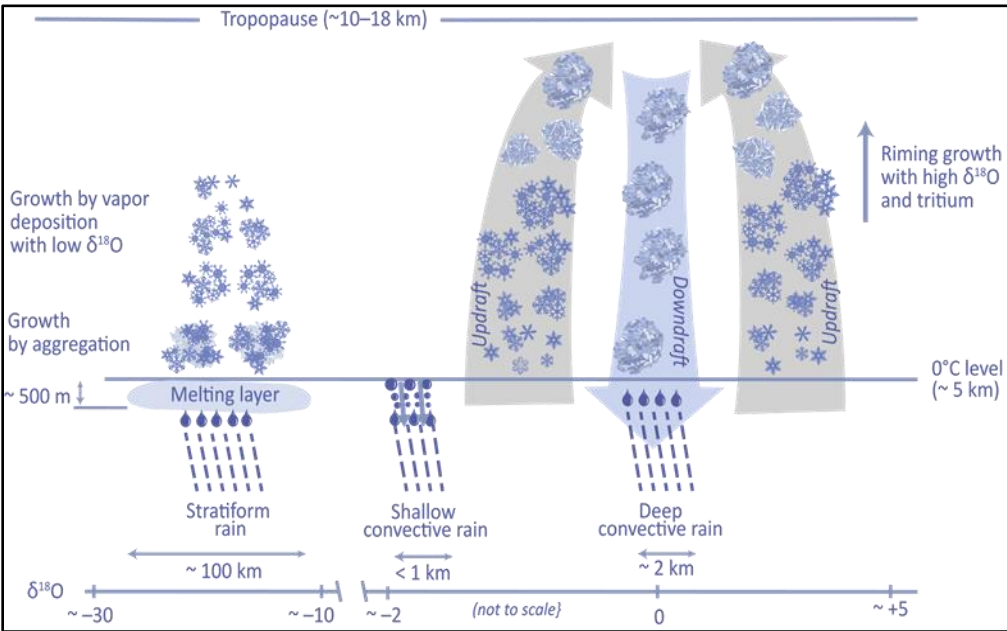
419

420

421 **Figure 1.** Correlation of mean monthly  $\delta^{18}\text{O}$ , stratiform fraction and precipitation amount in tropical  
 422 and midlatitude precipitation. The remainder of the rain fraction is convective (Methods). Solid line in  
 423 panel a) is based on a linear regression of all data points shown. The vertical axis in c) is shown in  
 424 reverse scale and trends in b) and c) are similar but opposite with respect to precipitation amount

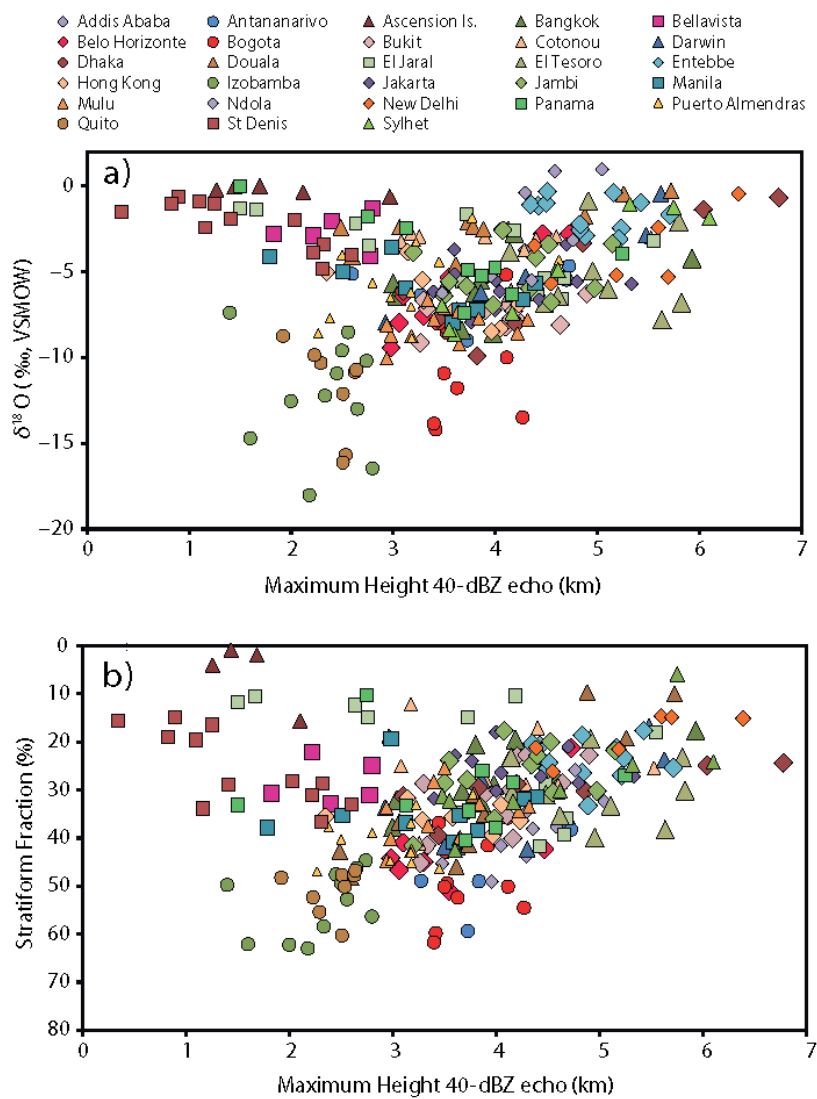


426 **Figure 2.** Schematic representation of differences in dynamical and microphysical processes in  
 427 convective and stratiform precipitation resulting in isotope variations. (Adapted after Houze Jr.<sup>18,19</sup>)  
 428  
 429  
 430



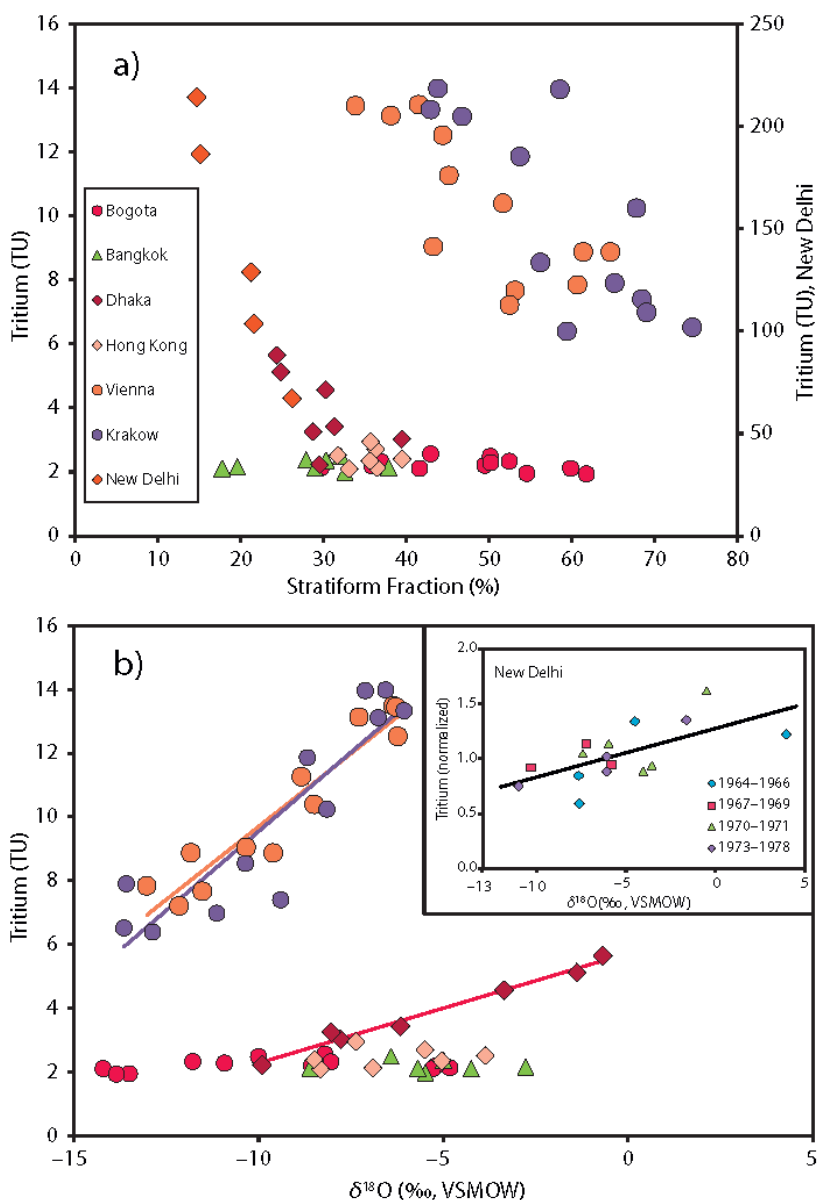
431  
 432  
 433

434 **Figure 3.** Correlation of mean monthly  $\delta^{18}\text{O}$  and stratiform fractions with the maximum height of 40-  
 435 dBZ echo. Precipitation with low stratiform fractions (or high convective fractions) has higher  $\delta^{18}\text{O}$  but  
 436 low or high echo heights reflecting shallow (warm rain) or deep convection.  
 437



438  
 439

440 **Figure 4.** Correlation of monthly precipitation tritium ( $^3\text{H}$ ) content with stratiform fractions and  $\delta^{18}\text{O}$ .  
 441 In 4a, note the much higher tritium at New Delhi because 1964-1978 data are used, while 2000-2012  
 442 data are used for the other stations. Tritium values in 4b-inset are normalized by the mean annual  
 443 average for each period (Methods). The New Delhi regression line has an  $R^2$  of 0.42 with  $p < 0.001$ .  
 444 Other regression lines have  $R^2$  of 0.81 (Krakow), 0.90 (Vienna), and 0.98 (Dhaka), all with  $p < 0.00001$ .  
 445



448  
449

**Table 1.** Geographical coordinates and related information for locations used in this study.

Code	Location	Lat.	Long.	Alt. (m)	Average Annual		Months with Precip > 50 mm*
					Precip (mm)	T (°C)	
6345000	Addis Ababa	9.00	38.73	2360	954	16.7	May-Sept
6708301	Antananarivo	-18.91	47.56	1295	1263	19.4	Jan-Apr; Nov-Dec
6190000	Ascension Is.	-7.92	-14.42	15	166	25.8	Mar-Aug
4845500	Bangkok	13.73	100.50	2	1661	28.5	Mar-Nov
8400101	Bellavista	-0.69	-90.33	194	763	22.5	Jan-May
8358301	Belo Horizonte	-19.87	-43.97	857	1190	22.5	Jan-Apr; Oct-Dec
8022200	Bogota	4.70	-74.13	2547	1029	13.3	Feb-Dec
9616301	Bukit (Sumatra)	-0.20	100.32	865	2005	21.9	Jan-Dec
6534403	Cotonou	6.42	2.33	14	1084	27.1	Mar-Jul; Sep-Nov
9412000	Darwin	-12.43	130.87	26	1902	27.3	Jan-Apr; Oct-Dec
4192300	Dhaka	23.95	90.28	14	1545	26.7	Apr-Oct
6491001	Douala	4.04	9.73	18	3787	27.2	Feb-Dec
7870802	El Jaral	14.94	-88.02	652	3586	22.6	Jan-Dec
8004401	El Tesoro	9.34	-75.29	175	1299	27.4	Mar-Dec
6370500	Entebbe	0.05	32.45	1155	1575	21.7	Jan-Dec
4500400	Hong Kong	22.32	114.17	66	2221	23.0	Apr-Oct
8404400	Izobamba	-0.37	-78.55	3058	1380	11.7	Jan-Jun; Aug-Dec
9674503	Jakarta	-6.29	106.67	45	1945	26.9	Jan-Sep; Nov-Dec
9619500	Jambi	-1.63	103.65	25	2126	26.9	Jan-Dec
9842900	Manila	14.52	121.00	14	1737	27.3	Apr-Dec
9644901	Mulu (Sarawak)	4.05	114.81	24	5026	27.0	Jan-Dec
6756100	Ndola	-13.00	28.65	1331	347	20.6	Jan-Feb; Nov-Dec
4218200	New Delhi	28.58	77.20	212	802	25.3	May-Oct
7880602	Panama	8.98	-79.53	5	1853	27.1	Apr-Dec
8437701	Puerto Almendras	-3.82	-73.38	98	3703	26.1	Jan-Dec
8407301	Quito	-0.17	-78.48	2789	808	15.2	Jan-May; Oct-Dec
6198001	St Denis	-20.90	55.48	70	1599	24.7	Jan-Dec
4190000	Sylhet	24.91	91.85	20	4012	25.7	Mar-Oct
1256500	Krakow	50.06	19.85	205	668	8.3	Jan-Dec
1103500	Vienna	48.25	16.36	198	684	10.3	Jan-Dec

450  
451  
452

\* except for Ascension Island, Vienna and Krakow, where all months with consistent data over multiple years were included.